Hanging Chain Vibration
MATH 485

3 May 2018

Cutillas, Philippe[1] and Engel, Lily[1] and Templin, Jasmin[1] and Granzier-Nakajima, Shawtaroh[1]

[1]Department of Mathematics, University of Arizona, Tucson AZ, 87521, USA

We verify and extend existing models of hanging chain vibration in two scenarios — oscillating in-plane, and rotating about a central axis. We implement Design of Experiments using a high-speed (1000 fps) camera to record chain shape and study differences between small and large vibration regimes. Models considered include nonlinear N-Pendulum, linear N-Pendulum, and classical small displacement model. We find classical and N-Pendulum models closely fit short-time behavior of experimental results in small vibration regime, but fail to capture the long-time friction damping behavior of experimental results; thus, we introduce linear Stokes's Drag term into models and fit a damping coefficient $k = 0.062$ kg/s. In large vibration regime, we find the non-linear N-Pendulum model closely fits short-time experimental results, but the nonlinear N-Pendulum model exhibits chaotic, unpredictable behavior not present in experimental results for long-time behavior. Hence, we propose a nonlinear N-Pendulum model with rotational damping to dampen fast moving chaotic behavior and better fit long-time experimental results.

1. Motivation & Background

Hanging chain problems continue to attract attention in physics and mathematics since James Bernoulli (1655-1705) first solved the case of a uniform chain hanging due to gravity [Wilson (1908)]. Hanging chains assume shapes of minimal bending stress; and thus, are ubiquitous in engineering applications such as the catenary shape in the design of archs. In some engineering applications such as the `Darrius turbine`, hanging chain shapes are used for turbine blade shapes. The Darrieus turbine has the shape of a troposkein which is the curve an idealized rope (in the absense of gravity) assumes when anchored at its ends and spun around its long axis at a constant angular velocity. The troposkien shape reduces the flatwise bending stresses due to centrifugal and gravitational forces as the blade tends to displace less from its original shape. A 1986 Sandia report discusses an improved model of the Darrieus turbine considering the shape a rope assumes under both rotation and the effects of gravity [Ashwill (1986)]. Thus, we are motivated to study the hanging chain in both in-plane and rotating context for possible engineering application.

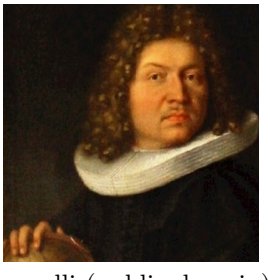

James Bernoulli (public domain)

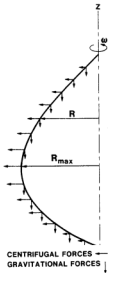

Darrius Turbin [Wacker (2005)]

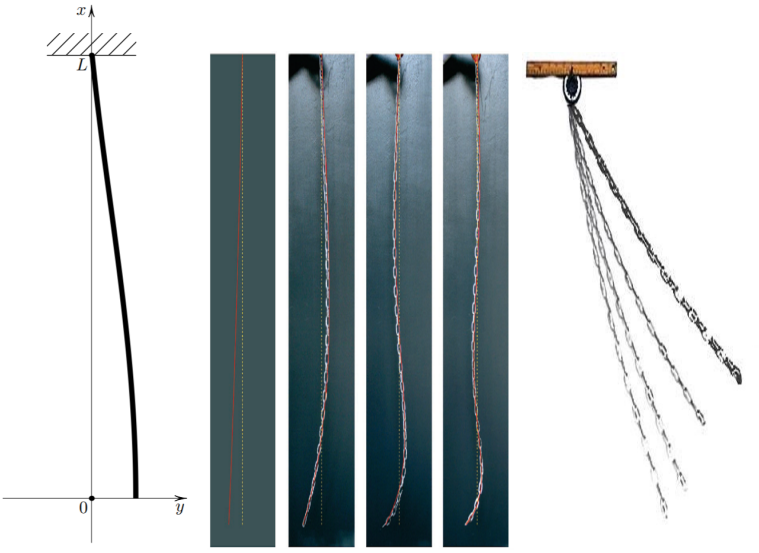

Figure 1: Model Small Oscillation [(Rozman 2017)], Large Oscillation

In the following section we develop three models to describe hanging chain vibration. First we present a classical solution which assumes small oscillation and displacement of the chain. Then we consider N-Pendulum as a bridge to model the hanging chain numerically, we develop both linearized and nonlinear models. Lastly, we perform experiments to verify these models and compare small oscillation regime to large oscillation regime.

.

Models

(i) Classical Small Displacement Model
(ii) Nonlinear N-Pendulum
(iii) Linear N-Pendulum

2. Model

2.1. *Classical Small Displacement Model*

The classical solution involves special functions, eigen-values, and separation of variables; thus, the problem is highly didactic of the methods involved and is presented in a number of classical mechanics textbooks [Morin (2003), McKay (2003)]. The hanging chain system presents an opportunity not only to contribute to novel research; but perhaps equally important, provides an opportunity contribute to the history of the problem's use in mathematical education. We develop the governing equation with newtonian physics. Fix the origin of our coordinate system at the un-fixed end of the chain (Figure 1). We consider displacement of the chain in the $\hat{\mathbf{x}}$ direction to be small relative to the length of the chain, L, and thus displacement, $\mathbf{u}$, is only considered in the in-plane $\hat{\mathbf{y}}$ direction and parameterized by vertical position x; and as such, we seek a model to describe u(x,t). Variables are defined as follows:

- u Transverse displacement $[m]$
- x Vertical height $[m]$
- t Time $[s]$
- ν Linear Density $[\frac{kg}{m}]$
- g Gravitational Acceleration $[\frac{m}{s^2}]$

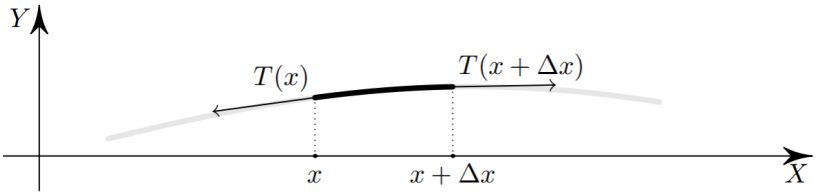

Figure 2: Hanging Chain.

Consider a small section of the chain of size Δx (Figure 2). We resolve forces in the $\hat{\mathbf{y}}$ direction, $\sum \mathbf{F} \cdot \hat{y} = m\mathbf{a} \cdot \hat{y}$, and take $\Delta x \to 0$ as follows,

$$\mathbf{T}(x + \Delta x) \cdot \hat{y} - \mathbf{T}(x) \cdot \hat{y} = \nu \Delta x \frac{\partial^2 u}{\partial t^2} \tag{2.1}$$

$$\lim_{\Delta x \to 0} \frac{\mathbf{T}(x + \Delta x) \cdot \hat{y} - \mathbf{T}(x) \cdot \hat{y}}{\Delta x} = \nu \frac{\partial^2 u}{\partial t^2} \tag{2.2}$$

$$\frac{\partial}{\partial x} \left\{ \mathbf{T}(x) \cdot \hat{y} \right\} = \nu \frac{\partial^2 u}{\partial t^2} \tag{2.3}$$

Observe that at an arbitrary point x in the chain, the vertical component of tension, $\mathbf{T}(x) \cdot \hat{x}$, must support the weight of the chain below it, $\nu g x$, thus $\mathbf{T}(x) \cdot \hat{x} = \nu g x$. Hence, we find $\mathbf{T}(x) \cdot \hat{y}$ by defining the angle between $\mathbf{T}$ and the $\mathbf{x}$ directions as θ. Further more, note that, since Tension is tangent to the chain, $\tan(\theta) = \frac{\partial u}{\partial x}$, thus, $\mathbf{T}(x) \cdot \hat{y} = \nu g x \frac{\partial u}{\partial x}$. Hence, returning to equation (2.3), we arrive at the governing equation,

$$\frac{\partial}{\partial x} \left[\nu g x \frac{\partial u}{\partial x} \right] = \nu \frac{\partial^2 u}{\partial t^2} \tag{2.4}$$

The chain is assumed to have uniform density and subject to a uniform gravitational field, thus g and ν are constants.

$$\frac{\partial^2 u}{\partial t^2} = g\left(\frac{\partial u}{\partial x} + x \frac{\partial^2 u}{\partial x^2}\right) \tag{2.5}$$

Next, we non-dimensionalize our equation. Let $X = \frac{x}{L}$, $U = \frac{u}{L}$, and $\tau = \frac{t}{\sqrt{\frac{g}{L}}}$. Thus, $X \in [0, 1]$, $U \in [0, 1]$, and $\sqrt{\frac{g}{L}}$ describes a characteristic time of the system, well known as the period of the simple pendulum. Substituting these variables yields the following non-dimensionalized governing equation and boundary condition

$$U_{\tau\tau} = U_X + X U_{XX}, \qquad U(1, \tau) \equiv 0. \tag{2.6}$$

For convenience, we switch back to conventional notation, with the understanding that we are working with the non-dimensionalized equation here-on-out unless otherwise stated, e.g.

$$u_{tt} = u_x + x u_{xx}, \qquad u(1, t) \equiv 0. \tag{2.7}$$

The rotating chain governing equation is identical to eq (2.7), except parameterized by displacement from the vertical axis $\hat{x}$, x, and arc-length, s [Yong (2006)], as follows

$$x_{tt} = u_s + s u_{ss}, \qquad u(1, t) \equiv 0. \tag{2.8}$$

We now use the method of separation of variables. We say that the solution U takes the

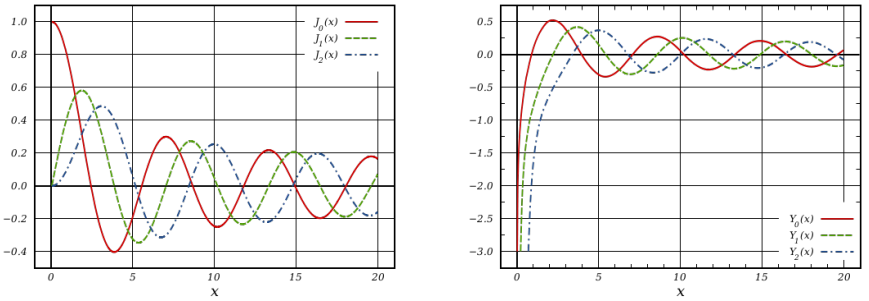

Figure 3: $J_0(x)$, $Y_0(x)$ [Byrne (2007)]

form $u(x,t) = X(x) \cdot T(t)$. Thus equation 2.7 reduces to the following.

$$\frac{T''}{T} = \frac{X' + x \cdot X''}{X} = -\lambda^2, \qquad \lambda \in \mathbb{R}. \tag{2.9}$$

In the standard way, the LHS and RHS are parameterized by different variables. The two are equal for all t and x, thus, both the LHS and RHS must equal some constant. Moreover, with foresight, we recognize that the LHS and RHS must equal some negative constant to avoid exponential and linearly growing time-dependent solutions. As a result, we arrive at the decoupled system,

$$T'' + \lambda^2 T = 0 \tag{2.10}$$

$$xX'' + X' + x^2\lambda^2 X = 0 \tag{2.11}$$

Solutions to the eq (2.9) are well known and describe oscillations of the form $\sin(|\lambda|t)$, $\cos(|\lambda|t)$. Letting $z^2 = 4x$ and using **chain** rule reduces eq (2.10) to,

$$z^2X'' + zX' + z^2\lambda^2 X = 0 \tag{2.12}$$

Eq (2.11) is well known as a zeroth order Bessel equation with linearly independent power series solutions J_0, Y_0 known as the Bessel functions of the first and second kinds respectively. These solutions can be found with Method of Frobenius [Byrne (2007)]. Hence the spacial profile is given by,

$$J_0(\lambda z) = J_0(2\lambda\sqrt{x}) \tag{2.13}$$

$$Y_0(\lambda z) = Y_0(2\lambda\sqrt{x})). \tag{2.14}$$

$Y_0(x)$ has an asymptote at $x = 0$ (see figure 3) which corresponds with the end of the chain and thus is un-physical hence we discard the Y_0 solution. By linearity, and the superposition principle, we arrive at the general solution,

$$u(x,t) = \sum_{n=0}^{\infty} \Big\{ A_n \sin(\lambda_n t) + B_n cos(\lambda_n t) \Big\} J_0(2\lambda_n\sqrt{x}). \tag{2.15}$$

Recalling the boundary condition, $u(1,t) = 0$, we get

$$\sum_{n=0}^{\infty} \Big\{ A_n \sin(\lambda_n t) + B_n cos(\lambda_n t) \Big\} J_0(2\lambda_n) = 0 \tag{2.16}$$

$$J_0(2\lambda_n) = 0 \tag{2.17}$$

For non-trivial result, A_n, $B_n \neq 0$, thus roots of J_0 determine natural frequencies λ_n. In

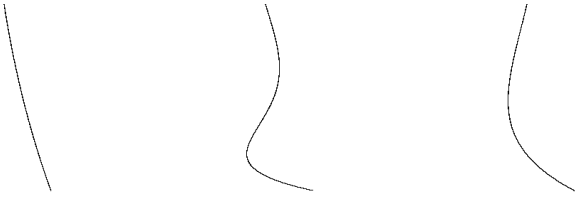

Figure 4: First Three Eigenfunctions Russell (2011)

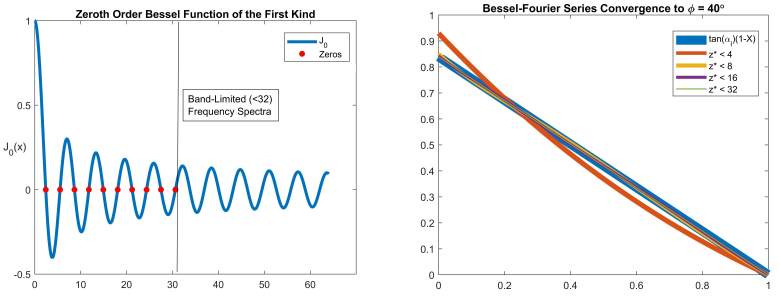

Figure 5: $J_0(x)$ (left), $u(x, t = 0)$ (right)

Figure 4, we present the first eigenfunctions corresponding with the first three zeroes of the Bessel function. A_n, B_n determined by initial conditions $u(x, t = 0), u_t(x, t = 0)$. In our experimental design (section 2.4), we consider the hanging chain released from rest, $u_t(x, t = 0) = 0$,

$$u_t(x, t = 0) = \lambda_n \sum_{n=0}^{\infty} \left\{ A_n \cos(\lambda_n t) - B_n \sin(\lambda_n t) \right\} J_0(2\lambda_n \sqrt{x}) \Big|_{t=0} = B_n$$

thus $B_n = 0$.

We find A_n by projecting onto a function space spanned by Bessel functions, where u_n corresponds with the n-th zero of J_0, under the following norm,

$$f(x) \sim \sum_{n=1}^{\infty} A_n J_0 \left(\frac{u_n}{x} \right) \qquad \langle f, g \rangle = \int_0^1 x f(x) g(x) \mathrm{d}x$$

Introduce the notation $(J_\alpha)_n(x) := J_\alpha \left(\frac{u_{\alpha,n}}{b} x \right)$. A series of the above form is known as a Fourier-Bessel series. Under the above norm, $\langle (J_\alpha)_m, (J_\alpha)_n \rangle = 0$ for $m \neq n$, thus, distinct $(J_\alpha)_n$ are orthogonal and thus, we determine the coefficients as follows,

$$\langle f, (J_0)_m \rangle = \langle \sum_{m=1}^{\infty} A_m (J_0)_n, (J_0)_n \rangle = A_m \langle \sum_{n=1}^{\infty} (J_0)_m, (J_0)_m \rangle$$

$$A_n = \frac{\langle f, (J_0)_n \rangle}{\langle (J_0)_n, (J_0)_n \rangle} = \frac{\int_0^1 x f(x) (J_0)_n(x) \mathrm{d}x}{\frac{1}{2} J_1^2(u_{0,n})}$$

For the purposes of this study, we consider initial conditions of the form $u(x, t = 0) = \tan(\alpha_i)(x-1)$ parameterized by release angle α_i. In Figure 5 we present the convergence of the Fourier-Bessel series to the initial condition showing that 10 terms, corresponding to the zeros left, are sufficient for convergence, and thus only 10 terms are used to calculate $u(x, t)$.

2.2. *Linear N-Pendulum*

The above section 2.1 presents the derivation of the small displacement assumption governing equation of the chain modeled as a continuum. In order to consider the dynamics of discrete links in a chain, we consider the N-Pendulum model (Figure 5). For our purposes, we consider the length of each pendulum arm l_i to be uniform $l_i = \frac{L}{N}$ where L is the total length of all the pendulum arms and N is the number of arms. Further, we consider each mass m_i to be uniform $m_i = \frac{M}{N}$ where M is the total mass. Moreover, to gain insight into the non-linear behavior of the hanging chain problem, we consider the non-linear N-pendulum system, in the next section (2.3), as a bridge to numerically study the behavior of the hanging chain without small displacement assumptions [Fritzkowski & Kaminski (2013), Wang (1994)].

We seek a model of N-coupled differential equations to describe the in-plane displacement of each mass, m_i. We apply Newtonian mechanics and conclude that the force on mass m_i is due moving pivot about mass m_{i-1} and the weight of the $N - i$ pendulum masses below.

$$F_i - F_{i-1} = m_i \ddot{u}_i \tag{2.18}$$

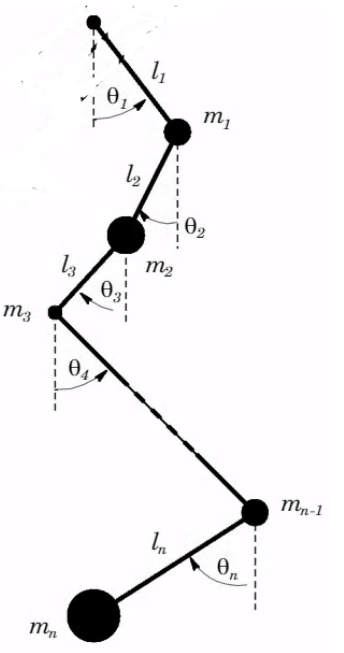

Figure 6: N-Pendulum Weibel & Baillieul (1998).

In a similar manner to the analysis in section 2.1, we observe that the vertical component of tension, $\mathbf{T_i} \cdot \hat{x}$, must support the weight of the chain below it, $\sum_{j=i+1}^{n} m_j g$, thus

$$\mathbf{T_i} \cdot \hat{x} = \sum_{j=i+1}^{n} m_j g \tag{2.19}$$

Hence, we find $\mathbf{T}(x) \cdot \hat{y}$ with θ_i as,

$$\mathbf{T_i} \cdot \hat{y} = \tan(\theta_i) \sum_{j=i+1}^{n} m_j g \tag{2.20}$$

Hence, returning to equation (2.18), we arrive at the governing equation,

$$\sum_{j=i+1}^{n} m_j g \tan(\theta_i) - \sum_{j=i}^{n} m_j g \tan(\theta_{i-1}) = m_i \ddot{u}_i \tag{2.21}$$

Note that each mass m_i is connected by fixed length pendulum arms. Thus, the above equation (2.20) determines the displacement in the $\hat{x}$ and simultaneously determines displacement in the $\hat{y}$ direction. We plan to use equation (2.20) to model the non-linear hanging chain system Wang (1994). We can further linearize equation (2.20) using small oscillations and displacement assumptions, $\theta_i << 1$ and $\frac{u_i}{L} << 1$ respectively. Using the

small angle approximation, $\tan(\theta_i) \approx \sin(\theta_i) = \frac{u_{i+1}-u_i}{l_{i+1}}$, we find (2.20) becomes

$$\sum_{j=i+1}^{n} m_j g \frac{u_{i+1}-u_i}{l_{i+1}} - \sum_{j=i}^{n} m_j g \frac{u_i - u_{i-1}}{l_i} = m_i \ddot{u}_i \tag{2.22}$$

Assuming equal, uniform mass and length, where $m_i = \frac{M}{N}$, $l_i = \frac{L}{N}$

$$\ddot{u}_i = \frac{g}{L/N}[(N-i)(u_{i+1} - 2u_i + u_{i-1}) - u_i + u_{i-1}]$$

Let $U = \frac{u}{L}$, $\tau = \frac{t}{\sqrt{\frac{g}{L}}}$. Thus $U \in [0,1]$ and $\sqrt{\frac{g}{L}}$ describes the characteristic time of the system, the same as we found in section (2.1). The non-dimension equation becomes,

$$U_{\tau\tau} = N[(N-i)(U_{i+1} - 2U_i + U_{i-1}) - U_i + U_{i-1}]$$

In matrix form,

$$\frac{d^2}{d\tau^2}\mathbf{U} = \mathbf{A}\mathbf{U} \tag{2.23}$$

where, $\mathbf{A}$ is tridiagonal given as,

$$\mathbf{A} = n \begin{bmatrix} 1-2N & N-1 & & & \dots & 0 \\ N-1 & 3-2N & N-2 & & \dots & \\ & N-2 & 5-2N & N-3 & \dots & \\ \vdots & \vdots & \vdots & \ddots & \vdots & \\ & & & 2 & -3 & 1 \\ 0 & & & & 1 & -1 \end{bmatrix} \tag{2.24}$$

The n-pendulum has been studied for unstable Inverted equilibria standing on its end and it has been found that the unstable equilbiria vanishes as $n \to \infty$ [Weibel & Baillieul (1998)]. Moreover, the natural frequencies approach zeroes of the Bessel function of the first kind. Hence, it appears the the N-Pendulum system does in-deed share characteristics with the hanging chain problem.

2.3. *Nonlinear N-Pendulum*

In order to model hanging chain behavior at large displacement, we develop a nonlinear N-Pendulum model without the small displacement and linearized assumptions in the above section 2.2. With the same variables and system (Figure 5), we proceed similarly using Newtonian mechanics [Dann *et al.* (2014)]. Consider the x_i, y_i components of each mass of the chain expressed via the angles θ_i, where $\frac{L}{N}$ is the length of each pendulum arm, we have,

$$y_n = \sum_{i=1}^{n} \frac{L}{N} \cos(\theta_i) \qquad\qquad x_n = \sum_{i=1}^{n} \frac{L}{N} \sin(\theta_i)$$

Differentiating once and twice yields the velocity and accelerations respectively,

$$\dot{y_n} = -\sum_{i=1}^{n} \frac{L}{N} \sin(\theta_i)\dot{\theta_i} \qquad\qquad \dot{x_n} = \sum_{i=1}^{n} \frac{L}{N} \cos(\theta_i)\dot{\theta_i}$$

$$\ddot{y_n} = -\sum_{i=1}^{n} \frac{L}{N} \left(\sin(\theta_i)\ddot{\theta_i} - \cos(\theta_i){\dot{\theta_i}}^2 \right) \qquad \ddot{x_n} = \sum_{i=1}^{n} \frac{L}{N} \left(\cos(\theta_i)\ddot{\theta_i} - \sin(\theta_i){\dot{\theta_i}}^2 \right)$$

Next we resolve forces and torques,

$$\sum_k F_{kX_i} = F_{x_i} - F_{x_(i+1)}$$

$$\sum_k F_{kY_i} = F_{y_i} - F_{y_(i+1)-mg}$$

$$\sum_k \tau_k = \frac{L}{N}(F_{yi}\sin(\theta_i) - F_{xi}\cos(\theta_i))$$

Next, we equate these forces and torques with inertial forces

$$m\ddot{x}_i = F_{x_i} - F_{x_(i+1)}$$

$$m\ddot{y}_i = F_{y_i} - F_{y_(i+1)-mg}$$

$$0 = \frac{L}{N}(F_{yi}\sin(\theta_i) - F_{xi}\cos(\theta_i))$$

For $i = n$, we have $F_{x(i+1)} = 0 = F_{y(i+1)}$, for $1 \leqslant i \leqslant n$, we have,

$$F_{xi} = \sum_{k=i}^{n} m\ddot{x}_k$$

$$F_{yi} = \sum_{k=i}^{n} m(\ddot{y}_k - g)$$

$$0 = \frac{L}{N}\left(\left(\sum_{k=i}^{n} m(\ddot{y}_k - g) \right) \sin(\theta_i) - \left(\sum_{k=i}^{n} m\ddot{x}_k \right) \cos(\theta_i) \right)$$

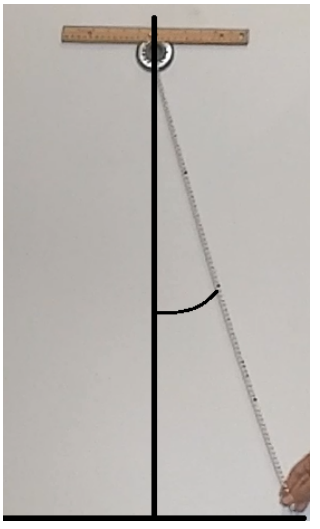

Figure 7: Experimental Setup

Substituting $\ddot{x_i}$, $\ddot{y_i}$, we have,

$$\begin{aligned}0 =& m\frac{L^2}{N^2}\cos(\theta_i)\Bigg(\sum_{k=i}^{n}\Bigg(\sum_{j=1}^{k}\Big(\sin(\theta_i)\dot{\theta_i}^{\,2} - \sin(\theta_i)\dot{\theta_i}^{\,2}\Big)\Big)\Bigg)\Bigg)\\ &- m\frac{L^2}{N^2}\sin(\theta_i)\Bigg(\sum_{k=i}^{n}\Bigg(\sum_{j=1}^{k}\Big(\cos(\theta_i)\dot{\theta_i}^{\,2} + \sin(\theta_i)\ddot{\theta}_i + g\Big)\Bigg)\Bigg)\\ =& \frac{L}{N}\Bigg\{ - mg(n-k)\sin(\theta_i) - m\sum_{k=i}^{n}\sum_{j=1}^{k}\frac{L}{N}\cos(\theta_i-\theta_j)\ddot{\theta_j} - m\sum_{k=i}^{n}\sum_{j=1}^{k}\frac{L}{N}\sin(\theta_i-\theta_j)\ddot{\theta_j}\Bigg\}\end{aligned}$$

Thus we have,

$$\mathbf{M}(\theta)\theta_{tt} + \mathbf{C}(\theta)\theta_t^2 + \mathbf{g}(\theta) = 0$$

where matrices $\mathbf{M}$, $\mathbf{C}$, and vector $\mathbf{g}$ are defined term-wise,

$$\mathbf{C}_{ij} = \frac{L}{N}(N - max(i,h))\sin(\theta_i - \theta_j)$$

$$\mathbf{M}_{ij} = \frac{L}{N}(N - max(i,h))\cos(\theta_i - \theta_j)$$

$$\mathbf{g}_i = g(N-i)\sin(\theta_i)$$

2.4. *Design of Experiments*

In-plane

To verify our models experimentally, we recorded in-plane hanging chain vibration modes with a Casio EX-FH25 High Speed Digital Camera. We did so for release angles of 10° to 90° in increments of 10, for both Mardi Gras beads and a chain. After recording these videos, we measured the horizontal displacement of 5 different points ($x = 0, \frac{L}{4}, \frac{L}{2}, \frac{3L}{4}, L$) on each chain, at times $t = \frac{T}{8}, \frac{T}{4}, \frac{3T}{8}$. Figure 7 presents the in-plane oscillation experimental set-up.

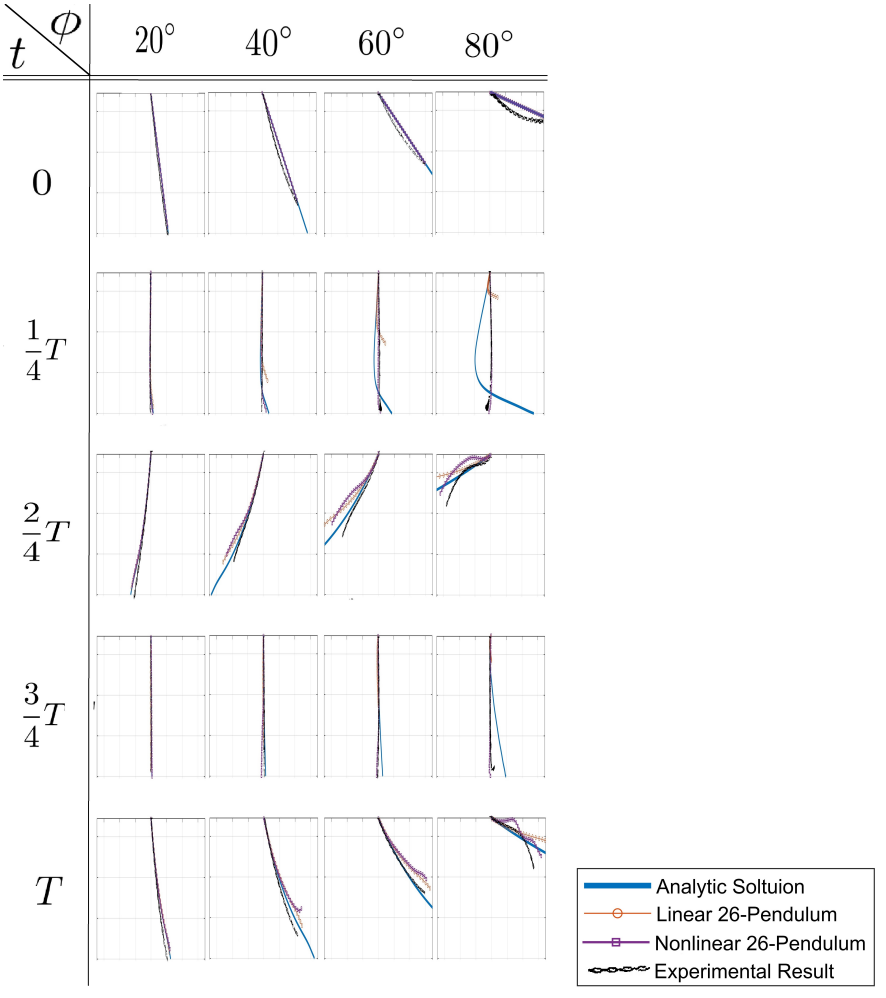

Figure 8: Analytic vs Numerical vs Experimental

3. Results

Below we present a plethora of videos of a variety of experimental and numerical results.

(i) **https://www.youtube.com/watch?v=GghLBtuXeJo**
(ii) **https://www.youtube.com/watch?v=6FqSx7l5anY**
(iii) **https://www.youtube.com/watch?v=sDRPPoG09b8**
(iv) **https://www.youtube.com/watch?v=aXSNzACZWh0**
(v) **https://www.youtube.com/watch?v=atpvWoE3YYw**
(vi) **https://www.youtube.com/watch?v=azpfJJz1aoU**

3.1. *In-Plane*

In the above Figure 8, we present a table plotting all models against the experimental results. At low angles we find all models are consistent, but at larger angles 60-80, we find that the non-linear model best fits the experimental results.

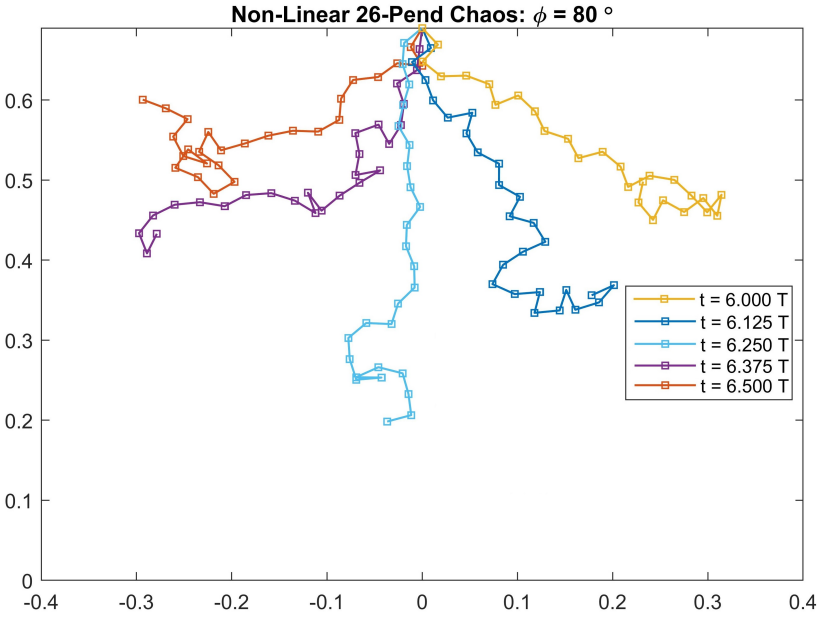

Figure 9: N-Pendulum Chaos

3.2. *Long Term Behavior*

In the above Figure 9, we present the chaotic behavior of the N-Pendulum model. Although the non-linear N-Pendulum model fit the experimental results at large oscillations best, the long term behavior of the model tended towards chaos. That is to say that long term behavior is sensitive to both initial conditions and subtle numerical error producing the unpredictable behavior in the above Figure 9. To dampen this chaotic behavior, we propose to add friction terms to prevent as dramatic and high velocity pendulum arms from whipping wildly in the N-Pendulum model, but also to model the long term experimental behavior of the chain which is to slowly decrease in amplitude over time (Figure 10). We propose to introduce a linear Stokes Drag term $-ku_t$,

$$U_{\tau\tau} = U_X + XU_{XX} - ku_t \qquad U(1,\tau) \equiv 0$$

Thus, upon separation of variables, the general solution takes the following form,

$$u(x,t) = e^{-\frac{k}{2}t} \sum_{n=0}^{\infty} \left\{ A_n \sin(\lambda_n' t) + B_n cos(\lambda_n' t) \right\} J_0(2\lambda_n \sqrt{x})$$

Where the natural frequency of the damped system is $\lambda_n' = \frac{1}{2}\sqrt{4\lambda_n^2 - k^2}$

We find with an exponential fitted curve (Figure 11) that the coefficient of friction of the chain we used is $k = .062$. Thus, since k is small, the system is under damped and the natural frequencies of the system are approximately the same as the original system.

$$\lambda_n' = \frac{1}{2}\sqrt{4\lambda_n^2 - k^2} \approx \lambda_n$$

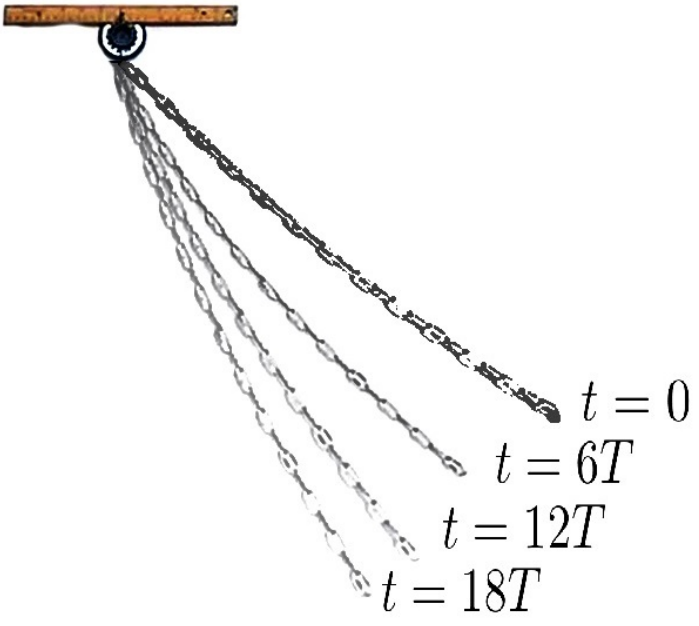

Figure 10: Air Drag

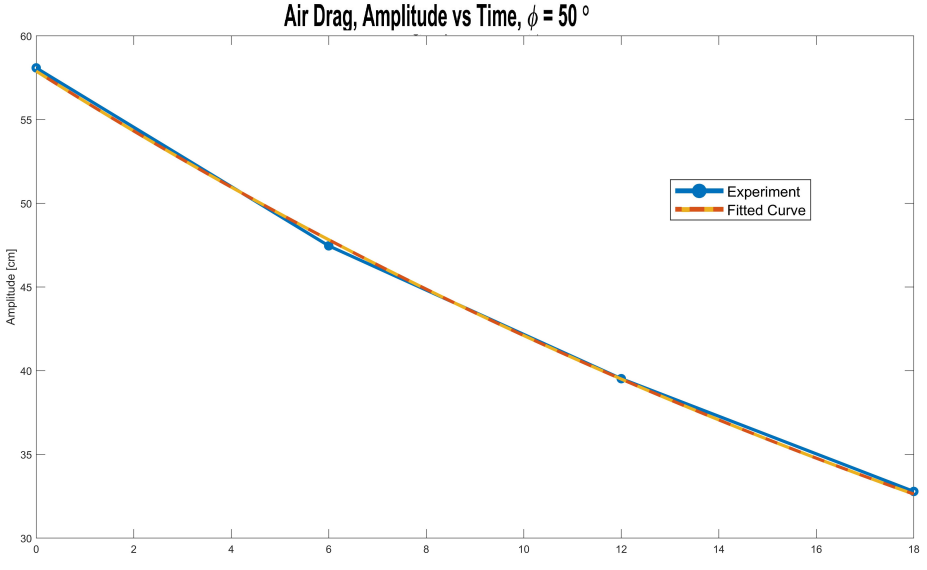

Figure 11: Air Drag

4. Rotation

In Figure 12, we present the fourth eigenfunction of the classical solution to equation (2.8), left, and the experimental result of slowly increasing the speed of rotation in a quasi-static regime, right. As the speed of rotation increases, the chain transitions to higher energy modes corresponding to the eigenfunction of the classical solution.

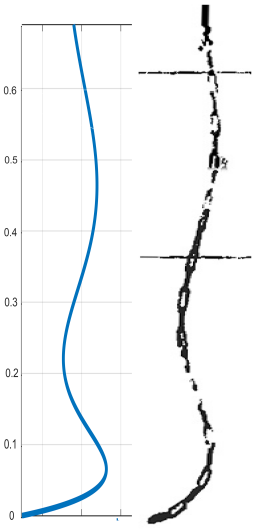

Figure 12: 4th Natural Frequency Mode of Analytic Solution (left), Experimental Rotating Chain (right)

5. Conclusions

• Analytic and numerical solutions closely fit experimental results for low release angles.

• Solutions deviated from experimental results for longer times and larger release angles.

• Extended model can be fit to experimental results using a coefficient of k= 0.062.

We find classical and N-Pendulum models closely fit short-time behavior of experimental results in small vibration regime, but fail to capture the long-time friction damping behavior of experimental results; thus, we introduce linear Stokes's Drag term into models and fit a damping coefficient $k = 0.062$ kg/s. In large vibration regime, we find the nonlinear N-Pendulum model closely fits short-time experimental results, but the nonlinear N-Pendulum model exhibits chaotic, unpredictable behavior not present in experimental results for long-time behavior. Hence, we propose a nonlinear N-Pendulum model with rotational damping to dampen fast moving chaotic behavior and better fit long-time experimental results.

There are an immense number of applications and extensions to apply to our basic model, and we list some here to perhaps motivate future projects. Some researchers have come across the self-knot phenomena. In the presence of large enough oscillations, the chain will overlap itself and essentially form a knot with itself [Belmonte (2001)]. Another interesting case to consider a magnetic chain [Schönke & Fried (2017)]. Other interesting applications include using a non-uniform density chain or material, using a driven system (eg. water hose), sliding the chain in addition to rotating it, and applying control theory stabilization methods. Using a buoyant material and attaching it at the bottom of our water-filled tank is also a variation of our original build that could provide some interesting results. However, it will be a challenge rigging a system in which we can use a drill to rotate the material in the tank from below.

6. Acknowledgments

This project is mentored by Loren Champlin, and high-speed camera and chain provided by Ildar Gabitov, whose help is acknowledged with great appreciation.

REFERENCES

Ashwill, Thomas D 1986 Developments in blade shape design for a darrieus vertical axis wind turbine. *Sandia Laboratorty* .

Belmonte, Andrew 2001 Dynamic patterns and self-knotting of a driven hanging chain. *Physical Review Letters* **87** (11).

Byrne, Charles 2007 Notes on bessels equation and the gamma function.

Dann, Christoph, Neumann, Gerhard & Peters, Jan 2014 Policy evaluation with temporal differences: A survey and comparison. *Journal of Machine Learning Research* **15**, 809–883.

Fritzkowski, P. & Kaminski, H. 2013 Non-linear dynamics of a hanging rope. *Latin American Journal of Solids and Structures* **10**, 81 – 90.

McKay, Benjamin 2003 *Lecture Notes: Partial Differential Equations for Engineers*. University of Utah.

Morin, David 2003 *INTRODUCTORY CLASSICAL MECHANICS*.

Rozman, Michael G. 2017 Lecture notes, oscillations of a hanging chain. *Department of Physics University of Connecticut* p. 1.

Russell, Daniel A. 2011 Acoustics and vibration animations.

Schönke, Johannes & Fried, Eliot 2017 Stability of vertical magnetic chains. *Proceedings of the Royal Society of London A: Mathematical, Physical and Engineering Sciences* **473** (2198), arXiv: http://rspa.royalsocietypublishing.org/content/473/2198/20160703.full.pdf.

Wacker, W 2005 A darrieus wind turbine has blades that approximate the shape of a troposkein to minimize bending stresses. *WikiMedia* .

Wang, C. Y. 1994 Stability and large displacements of a heavy rotating linked chain with an end mass. *Acta Mechanica* **107** (1), 205–214.

Weibel, Steven P. & Baillieul, John 1998 Open-loop oscillatory stabilization of an n -pendulum. *International Journal of Control* **71** (5), 931–957, arXiv: https://doi.org/10.1080/002071798221641.

Wilson, Edwin Bidwell 1908 The equilibrium of a heavy homogeneous chain in a uniformly rotating plane. *Annals of Mathematics* **9** (3), 99–115.

Yong, Darryl 2006 Strings, chains, and ropes. *SIAM Review* **48** (4), arXiv: https://doi.org/10.1137/050641910.